Second-Order Theory and Setup in Surface Gravity Waves: A Comparison with Experimental Data

A. TOFFOLI,*,& M. ONORATO,+ A. V. BABANIN,# E. BITNER-GREGERSEN,@ A. R. OSBORNE,+ AND J. MONBALIU*

*Katholieke Universiteit Leuven, Leuven, Belgium
+ Universitá di Torino, Turin, Italy
# Swinburne University of Technology, Hawthorn, Australia
@ Det Norske Veritas, Høvik, Norway

(Manuscript received 23 May 2006, in final form 5 December 2006)

ABSTRACT

The second-order, three-dimensional, finite-depth wave theory is here used to investigate the statistical properties of the surface elevation and wave crests of field data from Lake George, Australia. A direct comparison of experimental and numerical data shows that, as long as the nonlinearity is small, the second-order model describes the statistical properties of field data very accurately. By low-pass filtering the Lake George time series, there is evidence that some energetic wave groups are accompanied by a setup instead of a setdown. A numerical study of the coupling coefficient of the second-order model reveals that such an experimental result is consistent with the second-order theory, provided directional spreading is included in the wave spectrum. In particular, the coupling coefficient of the second-order difference contribution predicts a setup as a result of the interaction of two waves with the same frequency but with different directions. This result is also confirmed by numerical simulations. Bispectral analysis, furthermore, indicates that this setup is a statistically significant feature of the observed wave records.

1. Introduction

Statistical properties of surface gravity waves are essential for engineering purposes, such as the prediction of wave forces and structural responses (see, e.g., Goda 2000). For many years, it has been common practice to model the sea surface at a fixed point as a Gaussian random process (linear wave theory; Ochi 1998). In nature, however, waves tend to behave differently; crests are higher and troughs are shallower than predicted by linear theory. Furthermore, the departure from Gaussian statistics increases when the waves become steeper or the water depth becomes shallower (Ochi 1998). Such deviations are critical for predictions of extreme waves. Extreme waves are rare, their statistical properties are poorly known, and therefore their probabilities are usually predicted on the basis of extrapolations of distributions obtained for regular waves. Extreme waves, however, are mostly steep and highly nonlinear, and therefore deviations from Gaussian statistics are expected. In this respect, addition of the high-order Stokes-type terms to the linear approximation results in a more accurate description of the surface elevation (Whitham 1974).

An expression for the second-order correction to the linear wave theory was proposed by Hasselmann (1962), Longuet-Higgins and Stewart (1962), Longuet-Higgins (1963), and Sharma and Dean (1981). In principle, the model is able to include the effects of wave steepness, water depth, and directional spreading with no approximation other than the truncation of a small-amplitude expansion to the second order. Explorations of this method for short-crested waves (see, e.g., Forristall 2000; Prevosto et al. 2000; Jensen 2005) have shown that statistical properties of second-order simulated time series agree relatively well with field measurements in both deep and intermediate water depth. Note, however, that if the waves are long crested and narrow banded, modulational instability can develop

& Current affiliation: Det Norske Veritas, Høvik, Norway.

Corresponding author address: Alessandro Toffoli, Det Norske Veritas, Veritasveien 1, 1322 Høvik, Norway.
E-mail: alessandro.toffoli@dnv.com

DOI: 10.1175/2007JPO3634.1

and, as a result, wave crests can be much larger than the ones predicted by the second-order model (Janssen 2003; Socquet-Juglard et al. 2005; Onorato et al. 2006). Analysis of low-frequency wave components (e.g., Herbers et al. 1994), moreover, showed that second-order theory could also accurately represent measured locally forced infragravity motions.

The second-order wave theory was also used by Walker et al. (2004) to analyze the so-called New Year's wave, measured in 1995 at the Draupner oil field (in the central North Sea). The experimental data were low-pass filtered, and it was recognized that under the wave packet that contains the extreme wave, an anomalous setup, instead of an expected setdown, was present. They concluded that this result was inconsistent with second-order theory and some new physics should be incorporated. However, Okihiro et al. (1992) have shown theoretically that, in particular directional conditions, wave groups can actually force bound infragravity waves, which are in phase with the group envelope; this would, in principle, yield a setup of the mean free surface.

In the present study, we discuss the behavior of the second-order low-frequency response, and in particular the formation of the setup under energetic wave groups in short-crested sea states. We will also elaborate on the contribution of long waves to the amplitude of the largest crests, and the consequent change of the form of the wave crest distribution. Field measurements from Lake George in water of finite depth are used to support this analysis.

The paper is organized as follows: we first begin with a rapid description of the second-order model, including some details on the nonlinear parameters that can be derived if the narrowband approximation is performed. In section 3, we briefly describe the observed wave fields as well as the numerical simulations that are used herein. For selected classes of nonlinearity, the distribution of observed wave elevations and crest amplitudes is compared with second-order predictions; the findings are presented in section 4. In section 5, we discuss the behavior of the low-frequency fluctuations in relation to numerical simulations and field experiments; a bispectral analysis of the low-frequency components is also presented. In section 6, the influence of the long-wave components on the wave crest distribution is shown. Some concluding remarks are presented in the last section.

2. The second-order wave theory

Under the hypothesis of irrotational, inviscid fluid with constant depth, it is straightforward to show that a first-order (linear) solution of the Euler equations for surface gravity waves (Whitham 1974) takes the following form:

$$\eta^{(1)}(\mathbf{x}, t) = \sum_{i=1}^{N} \sum_{l=1}^{M} a_{il} \cos[k_i(x \cos\vartheta_l + y \sin\vartheta_l) - \omega_i t + \varepsilon_{il}], \tag{1}$$

where t is time, $\mathbf{x} = (x, y)$ is the position vector, ω_i is the angular frequency, θ_l is the wave direction, and ε_{il} is the phases; k_i is related to frequency through the linear dispersion relation $\omega_i = \sqrt{gk_i \tanh(k_i h)}$; N is the total number of frequencies and M is the total number of directions considered in the model; and a_{il} are the spectral amplitudes, which are calculated as follows:

$$a_{il} = a(\omega_i, \vartheta_l) = \sqrt{2E(\omega_i, \vartheta_l)\Delta\omega\Delta\vartheta}, \tag{2}$$

where $E(\omega_i, \vartheta_l)$ is the spectral density function. Note that Hasselmann (1962) also considered the random variation of the amplitudes in order to look in a proper statistical framework. By performing a few tests considering the amplitudes as random and deterministic variables, no significant differences were found in the probability distribution of normalized crest heights, which, for the linear case, fits the Rayleigh distribution. This is in agreement with Forristall (2000), who indicated that if a directional sea is simulated, the addition of different directional components, each with a random phase, at the same frequency automatically restores the statistical variability of the amplitudes.

The second-order correction to the linear wave surface [Eq. (1)] has the following form (see Sharma and Dean 1981):

$$\eta^{(2)}(\mathbf{x}, t) = \frac{1}{4} \sum_{i,j=1}^{N} \sum_{l,m=1}^{M} a_{il} a_{jm} [K^{-}_{ijlm} \cos(\varphi_{il} - \varphi_{jm}) + K^{+}_{ijlm} \cos(\varphi_{il} + \varphi_{jm})], \tag{3}$$

where $\varphi_{il} = k_i(x \cos\theta_l + y \sin\theta_l) - \omega_i t + \varepsilon_{il}$, and K^{+}_{ijlm} and K^{-}_{ijlm} are the coefficients of the sum and difference contributions. Their analytical expressions are reported in the appendix. Details concerning numerical aspects can be found in Sharma and Dean (1981), Dalzell (1999), and Forristall (2000).

Nonlinear parameters

When the water depth decreases the wave steepness is no longer the appropriate parameter to characterize the nonlinearity of the waves. To have some perspective on the relevance of the second-order contribution, it is instructive to look at the monochromatic limit, that is, $k_i = k_j = k$ and $\theta_l = \theta_m = 0$, of the coefficients K^{+}

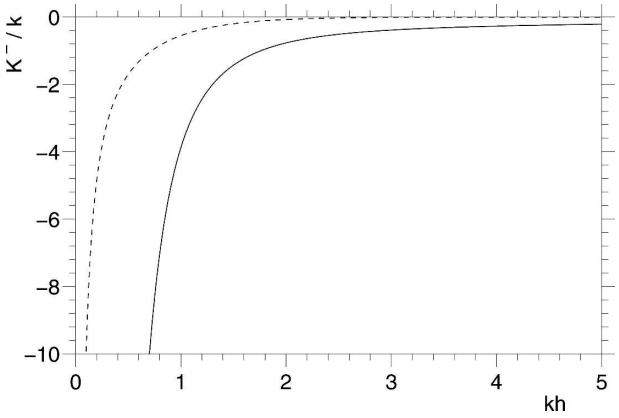

FIG. 1. Coupling coefficient K^-/k for a monochromatic wave considering the D^- term (solid line) and ignoring the D^- term (dashed line).

and K^- [Eqs. (A1)–(A7)]. For K^+ the calculation is straightforward and leads to

$$K^+ = \frac{k[4\tanh(kh) + \tanh(2kh)][1 - \tanh(kh)^2]}{\tanh(kh)[2\tanh(kh) - \tanh(2kh)]} + 2k\tanh(kh). \quad (4)$$

The same coefficient, expressed in a different manner, can be found in Whitham (1974). As $kh \to \infty$, it is easy to verify that $K^+ = 2k$, while for $kh \to 0$, then $K^+ = 3k/(kh)^3$. For K^- the calculation is a little bit more involved, because the direct substitution of $k_i = k_j = k$ and $\theta_l = \theta_m = 0$ leads to an undetermined form of D^- in Eq. (A4). Therefore, it is necessary to consider the case of $k_i = k_j + \delta$ and then take the limit for $\delta \to 0$. This calculation can be performed by taking the Taylor expansion of the numerator and the denominator in Eq. (A4) around $\delta = 0$. The final form for K^- is the following:

$$K^- = \frac{16k\cosh(kh)^2[4kh + \sinh(2kh)]}{-1 + 8(kh)^2 + \cosh(4kh) - 4kh\sinh(4kh)}. \quad (5)$$

Similar expressions for the second-order difference contribution (K^-) also can be found in Whitham (1974), Martinsen and Winterstein (1992), Prevosto et al. (2000), and Janssen and Onorato (2005). As $kh \to \infty$, it is easy to verify that $K^- = -k/(kh)$, while for $kh \to 0$ then $K^- = -3k/(kh)^3$. It is important to note that if the contribution from D^- is ignored, then $K^- = -2k/\sinh(2kd)$. This latter expression for low-frequency contribution has been used in the past (see, e.g., Forristall 2000) to include the setdown in the Tayfun (1980) distribution in finite depth. In Fig. 1, we show these two forms of K^-/k as a function of the relative depth kh; the correct expression of K^- [Eq. (5)], shown as a solid line, tends to zero very slowly as the water depth increases.

As a result of the monochromatic approximation, the surface elevation can be written as a second-order Stokes series:

$$\eta(x, t) = \frac{1}{4}a^2K^- + a\cos(\psi) + \frac{1}{4}a^2K^+\cos(2\psi), \quad (6)$$

with $\psi = kx - \omega t$. Two nonlinear parameters, which measure the relevance of the second-order contribution, can be identified. The first one is given by the ratio of the amplitude of the higher harmonic to the amplitude a of the main wave:

$$\mu' = \frac{1}{4}aK^+. \quad (7)$$

For deep-water waves $\mu' = ka/2$, and therefore is proportional to the wave steepness; in the shallow-water regime, $\mu' = 3ka/(4k^3h^3)$, which is the Ursell number (Ursell 1953; see also Osborne and Petti 1994). To characterize our experimental data, in the rest of the paper we will use a parameter given by $\mu = 2\mu'$; this is simply because in deep water μ reduces exactly to the wave steepness of a monochromatic wave, that is, $\xi = ka$.

The second nonlinear parameter is given by the ratio of the amplitude of the low-wavenumber contribution to a:

$$\nu = \frac{1}{4}a|K^-|. \quad (8)$$

It is clear that the Stokes series, Eq. (6), is convergent if both nonlinear parameters are small, therefore, these two parameters can furnish a first guess on the relevance of the second-order contributions in experimental data.

3. Datasets: Field measurements and numerical simulations

Surface elevations are taken from an integrated set of measurements, which were carried out at the Lake George field experimental site (Australia) from September 1997 to August 2000 (see Young et al. 2005 for details). The observations were collected by means of a spatial array of eight capacitance gauges sufficiently far from any disturbances at the sampling frequency of 25 Hz; for this analysis the original records have been subdivided in 15-min time series.

The lake bottom in the region of the observation site is very flat. As the lake was drying out, following its natural cycle, the water depth gradually changed from 1.1 m in the beginning of the measurements down to

0.4 m by the end of the experiment in year 2000. Under typical meteorological conditions the range of the relative depth kh was mainly representative of a deep and intermediate water depth wind sea. The degree of nonlinearity, as measured by μ, varies from a minimum of about 0.14 for $kh \gg 1$ up to 0.70 for $kh \approx 0.70$. Note that μ has been defined in the previous section for a monochromatic wave; for random waves we have used $a = H_s/2$, where H_s is the significant wave height of each individual time series, and $k = 2\pi/\lambda_p$, where λ_p is the wavelength related to the peak period.

To describe the wave field at Lake George, we chose to approximate the spectral density function with the Joint North Sea Wave Project (JONSWAP) formulation (Komen et al. 1994), because it is most frequently used for a variety of applications. According to the spectral parameters and the spectral form of the measured records, we construct a JONSWAP-like spectrum with a peak period of $T_p = 1.8$ s, a peak enhancement factor of $\gamma = 2.0$, and a Phillips parameter of $\alpha = 0.02$ to provide an average description of the observed spectra; these parameters correspond to a significant wave height $H_s = 0.23$ m. The directional distribution can be expressed by a $\cos{-2s}$ function (e.g., Hauser et al. 2005), where the s coefficient is evaluated as follows:

$$s(\omega) = \begin{cases} 11\left(\dfrac{\omega}{\omega_p}\right)^{2.7} & \omega < \omega_p \\ 11\left(\dfrac{\omega}{\omega_p}\right)^{-2.4} & \omega \geq \omega_p \end{cases}, \tag{9}$$

where $\omega_p = 2\pi/T_p$ is the peak angular frequency. The expression of s [Eq. (9)] was derived by Young et al. (1996), who used a maximum likelihood method to fit Lake George's data (measured from April 1992 to October 1993) to the analytical form of the spreading function.

These spectral distributions are used herein as input to simulate directional surface elevations at a fixed point {for convenience we assume $\mathbf{x} = [0, 0]$}. A first-order description of the sea surface is initially calculated from Eq. (1), choosing the phases ε from a uniform random distribution in the interval $[0, 2\pi]$ and using an inverse fast Fourier transform to perform the summations in Eq. (1). The second-order corrections are then calculated for each pair of wave components using the summations in Eq. (3). Different degrees of nonlinearity are achieved by performing the simulations at several water depths. Table 1 illustrates the different relative water depths and nonlinear parameters (ξ, μ, and ν) that were taken into account.

Repeating a simulation many times with different random phases for the same spectral density and water depth gives enough samples to stabilize the statistics at low probability levels. In a typical run, we would produce 500 repetitions with 2048 time steps at the sampling frequency of 25 Hz (approximately 25 000 waves); an angular resolution of 12° is used for these simulations.

TABLE 1. Relative water depths kh, wave steepness ξ, nonlinear parameter μ, and second-order difference contribution ν.

kh	ξ	μ	ν
1.75	0.14	0.19	0.04
1.52	0.15	0.22	0.05
1.39	0.15	0.25	0.07
1.29	0.16	0.28	0.08

4. The distribution for surface elevation and wave crests

The form of the statistical distribution changes according to the values of the nonlinear parameters μ and ν. In the following, we investigate whether this behavior is captured by the second-order simulations for increasing nonlinearity. Because often the extreme values have an important role in applications, we concentrate this analysis on the tail of the statistical distribution.

In the remainder of the paper, it is convenient to normalize the surface elevation by means of the standard deviation $\sigma = \sqrt{m_0}$, where m_0 is the spectral variance. The statistical distributions of the simulated and measured wave elevation and crest amplitude are presented in Figs. 2 and 3. Note that we compare datasets with equivalent nonlinearity. We have, therefore, classified the field observations into groups on the basis of the nonlinear coefficient μ; for the present analysis, only those 15-min time series that fall within the following classes are considered: $0.17 \leq \mu < 0.20$, $0.20 \leq \mu < 0.23$, $0.23 \leq \mu < 0.26$, and $0.26 \leq \mu < 0.29$. For each class we take approximately 25 000 waves to be consistent with the number of simulated waves.

We first consider the distribution of the surface elevation η/σ. For a relatively low value of the nonlinear parameter, that is, $\mu = 0.19$, the second-order simulations approximate the measurements well. As the nonlinearity increases, the crests become sharper and higher while the troughs become broader and less deep. For $\mu = 0.22$ and $\mu = 0.25$, the changes of the upper tail of the distribution seem to be captured by the second-order interactions, though a departure of the lower tail increases in magnitude as the value of the nonlinear parameter increases. At a degree of nonlinearity as high as $\mu = 0.28$ (Fig. 2, bottom-right panel), the simulations generate negative displacements up to 15%

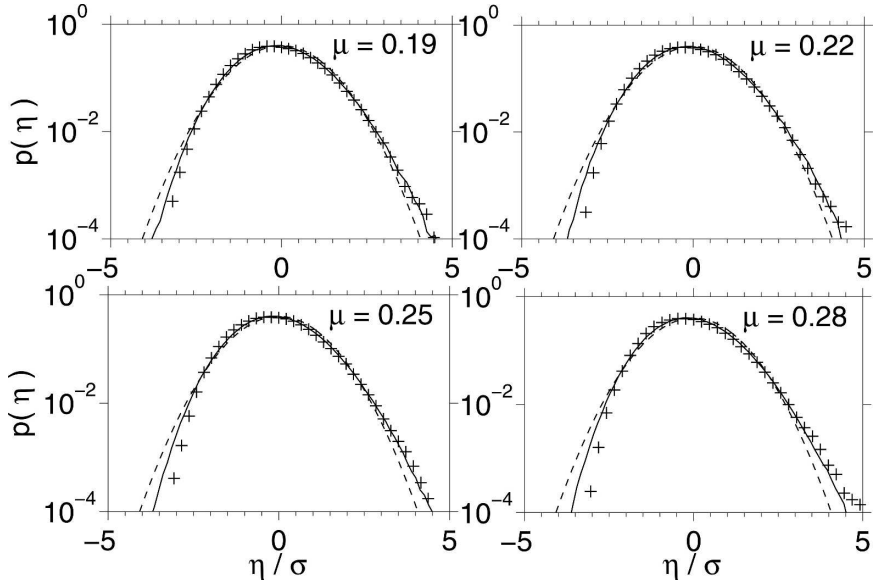

FIG. 2. Statistical distribution of second-order dimensionless wave elevations (solid line) compared with the Gaussian probability density function (dashed lines) and field measurements (+).

deeper than those of the measurements. In addition, a deviation of the upper tail of the distribution also becomes visible.

We then investigate the statistical distribution of the crest amplitude (η_c/σ), which we define as the maximum elevation of an individual wave (IAHR Working Group on Wave Generation and Analysis 1986). For a degree of nonlinearity equivalent to $\mu = 0.19$ and $\mu = 0.22$, the second-order truncation of a Stokes expansion provides an adequate description of the observations (see Fig. 3, top panels). A departure from the simulations, however, becomes visible for a degree of nonlinearity as $\mu = 0.25$, and increases in magnitude as the nonlinearity is enhanced (Fig. 3, bottom panels). To

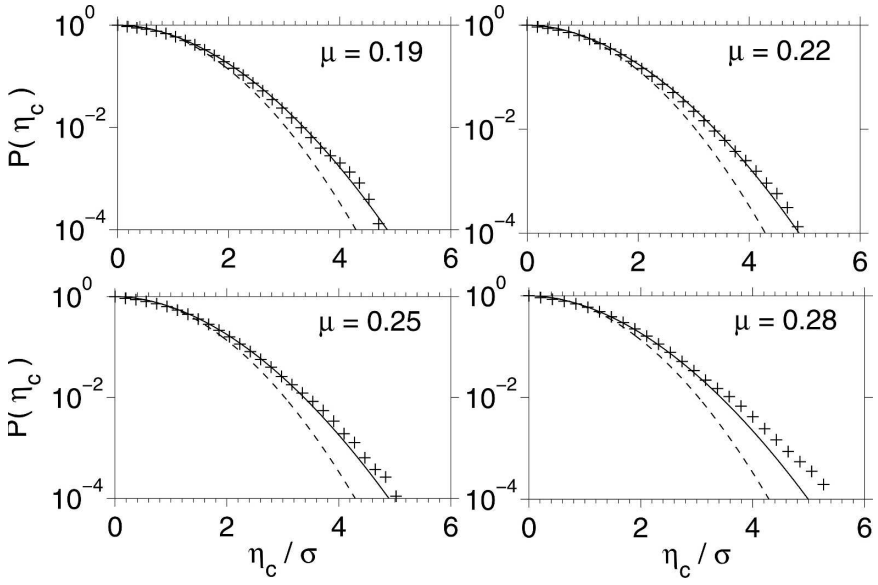

FIG. 3. Statistical distribution of second-order dimensionless crest amplitudes (solid line) compared with the Rayleigh probability density function (dashed lines) and field measurements (+).

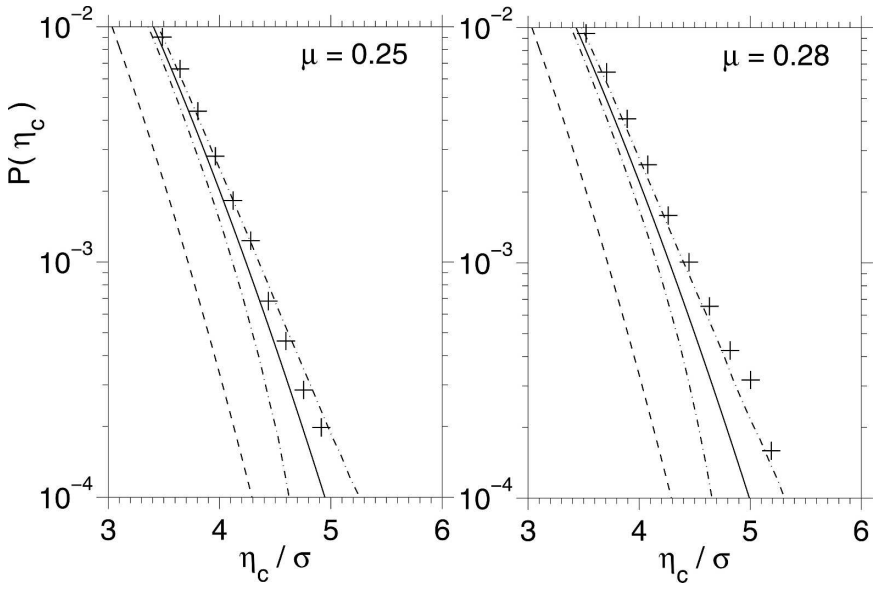

FIG. 4. Bootstrap uncertainty of the simulated wave crest distribution: second-order crest distribution (solid line), Rayleigh probability density function (dashed line), 95% confidence limits (dash–dot line), and field measurements (+).

measure whether this deviation is statistically significant, we have estimated the confidence limits for the statistical distribution of the simulated amplitudes by means of a bootstrap technique. This method is a resampling procedure, which provides random copies of the original dataset (see Emery and Thomson 2001 and references therein). For each bootstrap sample, the statistical properties, that is, wave crest distribution, can be recomputed; repeating this process many times (typically 1000), the asymptotic 95% confidence interval for the probability density function can be evaluated. The tail of the second-order wave crest distribution and the related uncertainty are presented in Fig. 4. At a degree of nonlinearity equivalent to $\mu = 0.25$, the distribution of the observed crests lays within the 95% confidence limits related to the simulated statistics (see Fig. 4, left panel); the deviation is not statistically significant. For values of the nonlinear parameter that overcome this threshold (e.g., $\mu = 0.28$ in this study), the error that one would make by approximating the observations with the second-order time series is larger than the uncertainty of the simulations. Note, however, that such a result is not totally unexpected, because the assumption of a small amplitude is not completely satisfied for $\mu \geq 0.28$.

To explain the observed deviation, it is instructive to look at the fourth-order moment of the probability density function, the kurtosis, which refers to extreme values (see, e.g., Mori and Janssen 2006). Although a Stokes expansion truncated at the second-order provides a good description of the third-order moment (i.e., skewness) of the probability density function (Martinsen and Winterstein 1992), it does not adequately represent the kurtosis (see Socquet-Juglard et al. 2005). For a degree of nonlinearity as $\mu = 0.25$, however, the observed kurtosis is, on average, close to the value that one would expect for Gaussian-distributed waves (i.e., linear waves). Because its contribution is therefore negligible, the second-order theory gives a proper statistical description of the observations (the deviation, in fact, is not statistically significant). For higher nonlinearity, however, the contribution of kurtosis becomes more relevant. Therefore, third-order terms should be added to the Stokes expansion in order to capture this enhancement, which is responsible for the significant deviation of the wave crest distribution observed for $\mu = 0.28$ (Fig. 4, right panel).

It is also important to note that the JONSWAP parameterization for the frequency spectrum may not be adequate in finite water depths, where high values of μ are expected. The probability distribution might assume a slightly different form if, for example, a Texel–Marsen–Arsloe (TMA) spectral formulation (Bouws et al. 1985) is used; this has not been investigated though.

5. The low-frequency nonlinear response

a. Behavior of the long-wave components

The most basic feature that one would expect from second-order interaction is the sharpening of the wave

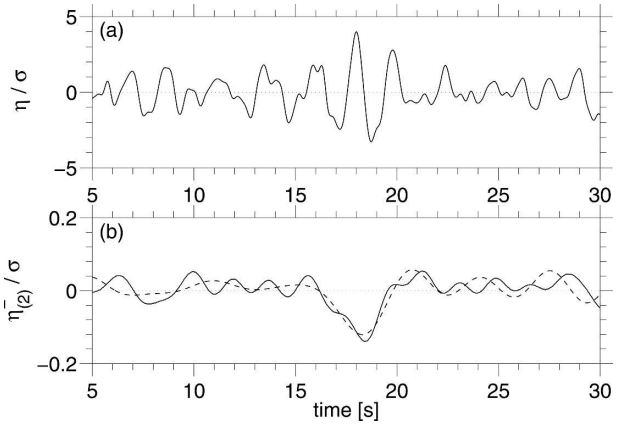

FIG. 5. Simulated (a) second-order wave profile and (b) low-frequency response: second-order difference contribution (solid line) and approximated low-frequency response (dashed line). The profile was simulated by using a JONSWAP-like spectrum (T_p = 1.8s, γ = 2.0, α = 0.020) and a cos−2s directional function; the degree of nonlinearity is μ = 0.25 (ν = 0.07).

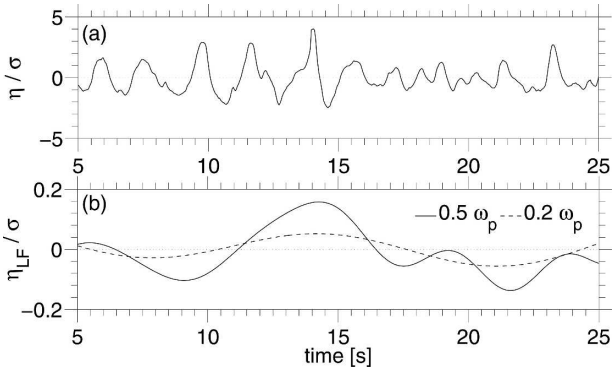

FIG. 6. Example 1 of setup under energetic groups of steep waves as measured at Lake George's instrumentation site: (a) measured profile and (b) filtered low-frequency components; degree of nonlinearity $\mu \approx 0.25$ ($\nu \approx 0.07$).

crests and the flattening of the wave troughs. This is expressed by the second-order sum contribution in Eq. (3), which occurs at the sum of the frequencies of the interacting wave components. But, the second-order interaction also generates a low-frequency response, which occurs at the difference of the frequencies and is phase coupled to the group envelope. For a narrow directional distribution, it is expected to depress the mean sea level, that is, it gives a setdown under the energetic groups, and to increase it elsewhere (Longuet-Higgins and Stewart 1962, 1964; Hasselmann et al. 1963; Elgar and Guza 1985; Okihiro et al. 1992; Herbers et al. 1994; Dalzell 1999). Thus, the wave envelope and low-frequency components result in a phase shift of π. An example of the second-order difference contribution is presented in Fig. 5 for a degree of nonlinearity μ = 0.25 (ν = 0.07); the profile was simulated by using a JONSWAP-like spectrum (T_p = 1.8 s, γ = 2.0, α = 0.02) and a cos−2s directional function, with s defined as in Eq. (9).

An estimation of the setdown can be extracted by low-pass filtering the wave signal with a cutoff frequency of $\omega \approx 0.5\ \omega_p$. The approximated low-frequency response is presented as a dashed line in Fig. 5b. The choice of the cutoff frequency is consistent with the work by Walker et al. (2004), who separated the second-order difference contribution from the measured records. In the remainder of the paper, this approximation will be used to represent the low-frequency response.

In nature, sometimes, the low-frequency components may behave differently from the second-order narrow-band prediction. Walker et al. (2004), analyzing the Draupner New Year wave (Haver and Andersen 2000), showed that the low-frequency contribution resulted in an elevation setup of the mean free surface under the largest wave height. The particular meteorological and oceanographic conditions at the time of the event and the bathymetry defined a nonlinear coefficient $\mu \approx$ 0.18; satellite measurements close to this location indicate that this event was fairly short crested (Nieto-Borge et al. 2004). Although unexpected, a similar feature can be extensively seen under many (but not all) energetic groups in Lake George's dataset. Despite the fact that it appears for any considered degree of nonlinearity, it is more common for high values of μ and ν, that is, $\mu \geq 0.25$ and $\nu \geq 0.07$. Two examples of the observed setup, which has been extracted by low-pass filtering the measured time series, are presented in Figs. 6 and 7 for nonlinearity $\mu \approx 0.25$ ($\nu \approx 0.07$). Filtering

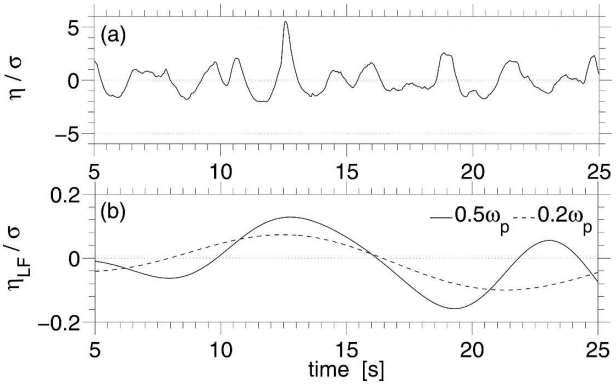

FIG. 7. Example 2 of setup under energetic groups of steep waves as measured at Lake George's instrumentation site: (a) measured profile and (b) filtered low-frequency components; degree of nonlinearity $\mu \approx 0.25$ ($\nu \approx 0.07$).

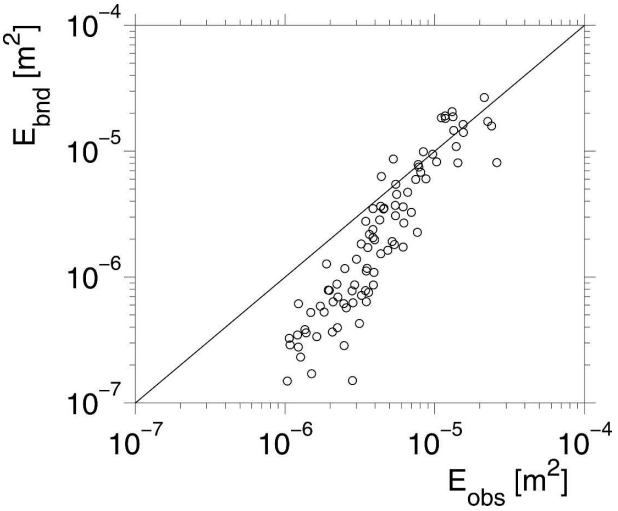

FIG. 8. Predicted infragravity (0.005–0.05 Hz) bound wave energy (E_{bnd}) vs total observed infragravity wave energy (E_{obs}).

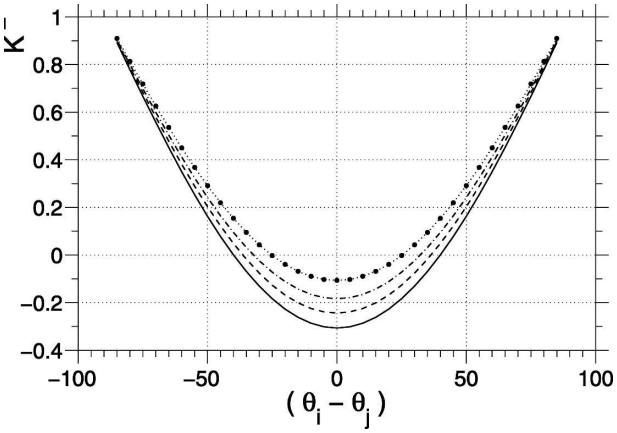

FIG. 9. Second-order negative interaction kernel (K^-) for two identical frequency ($\omega_i = \omega_j = \omega_p$) with different directions: kh = 1.75 (dotted line); kh = 1.52 (dash–dot line); kh = 1.39 (dashed line); kh = 1.29 (solid line).

with progressively lower cut-off frequencies (see, e.g., Figs. 6b and 7b) confirms the robustness of this feature.

It is important to note that free infragravity waves (0.005–0.05 Hz), such as radiated long waves from the nearby coast, can contaminate the low-frequency range well offshore (see Okihiro et al. 1992; Herbers et al. 1994, 1995). Because these waves are no longer forced by wave groups, namely, free infragravity waves are not phase coupled, they may be responsible for the setup of the mean free surface (see, e.g., Battjes et al. 2004, and references therein), if they dominate the infragravity frequency band. To understand the role of free infragravity waves in the observed time series, we have compared the total, observed, infragravity energy E_{obs} with predictions of infragravity, second-order (bound) energy E_{bnd} (cf. Herbers et al. 1994); observed and predicted energies in the infragravity frequency band are calculated as follows:

$$E_{\text{obs}} = \int_{\omega_1}^{\omega_2} d\tilde{\omega} \int_0^{2\pi} E(\tilde{\omega}, \theta)\, d\theta \quad \text{and} \tag{10}$$

$$E_{\text{bnd}} = 2 \int_{\omega_1}^{\omega_2} d\tilde{\omega} \int_{\tilde{\omega}}^{\infty} d\omega \int_0^{2\pi} d\theta_1 \int_0^{2\pi} (\text{K}^{-2}) \times (\omega + \tilde{\omega}, \omega, \theta_1, \theta_2) E(\omega + \tilde{\omega}, \theta_1) E(\omega, \theta_2)\, d\theta_2, \tag{11}$$

where $\omega_1 < \tilde{\omega} < \omega_2$ is the infragravity range expressed in angular frequency, and $E(\omega, \theta)$ is the measured directional spectrum, which is calculated from the wave records by using the maximum likelihood method (see Young et al. 1996 for details). In Fig. 8, the total and predicted infragravity energies are compared.

Predicted infragravity bound energy (E_{bnd}) approximates the total infragravity energy (E_{obs}) well if surface gravity waves are very energetic; namely, bound waves dominate the infragravity frequency range. If the energy level is small, however, free infragravity waves contaminate the low-frequency band. Consequently, the predicted infragravity bound waves underestimate the total infragravity energy. Nonetheless, because bound waves contribute, on average, to 60% of the total energy in the infragravity frequency range, we can conclude that the influence of free infragravity waves on the formation of the setup should be marginal.

b. *Influence of the directional distribution*

Okihiro et al. (1992), Herbers et al. (1994), and Dalzell (1999) showed that the second-order interaction between different directional components could substantially influence the behavior of the low-frequency response. In Fig. 9, we show the values that the second-order difference contribution [Eq. (A2)] assumes for different relative depths, when the interacting wave components have identical frequencies, $\omega_i = \omega_j = \omega_p$, and different directions, $\vartheta_l \neq \vartheta_m$. The difference contribution coefficient K^- [Eq. (A2)], in particular, reaches positive, large values as the interacting wave components propagate with well-separated directions. In general, for a certain degree of nonlinearity and a common analytical form of the directional spreading [e.g., the $\cos{-2s}$ function with s defined as in Eq. (9)], the contribution of the different directional compo-

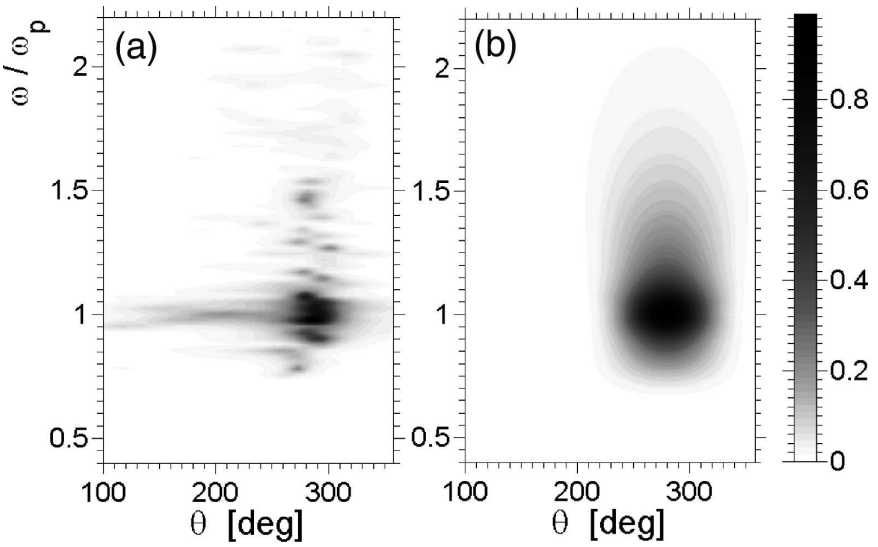

FIG. 10. Example of (a) broad directional wave spectrum at Lake George and (b) analytical spectrum; degree of nonlinearity $\mu \approx 0.25$ ($\nu \approx 0.07$). The spectra are normalized by using the concurrent energy peaks.

nents results in a substantial reduction of the amplitude of the setdown (Dalzell 1999; Toffoli et al. 2006). However, the second-order low-frequency response could also produce a positive elevation of the mean sea level, that is, setup, under energetic wave groups if a more directionally spread spectrum is considered (see Okihiro et al. 1992). For example, Toffoli et al. (2006) obtained such a result by performing second-order simulations of a bimodal wave field, which was defined by two identical JONSWAP-like spectra (with a very narrow directional spreading) with mean wave directions, such that $\overline{\vartheta}_1 - \overline{\vartheta}_2 = 90°$. In this condition, the second-order subharmonics were observed to be in phase with the wave envelope.

In Lake George, the actual directional spreading can differ from the analytical form, which was chosen to perform the simulations; the latter, in fact, only represents an average description of Lake George's wave field. The records used for this analysis, for example, show a relatively broader directional spreading than the one predicted by Eq. (9) at the energy peak. In Fig. 10, we compare, as an example, a directional wave spectrum observed for $\mu \approx 0.25$ ($\nu \approx 0.07$) and the analytical form of the directional spectrum. In particular, the increase of the nonlinear coupling between wave pairs in finite water depth (this corresponds to high values of μ and ν in this work) can result in an enhancement of the directional spreading of the wave spectra (Young et al. 1996). Thus, the actual directional distribution, in some particular cases, may be more directionally spread than the analytical representation (Fig. 10). Such directional patterns, therefore, can be responsible for the generation of the observed setup.

To validate this hypothesis, second-order time series have been simulated by using progressively broader input spectra but an identical phase ε. At the peak frequency, Eq. (9) provides a directional spreading $s(\omega_p) = 11$; herein, we use a modified form of Eq. (9), such that $s(\omega_p) = 7$, 5, and 3. Note that directional spreading with $s(\omega_p) \leq 5$ was rather common at Lake George (see, e.g., Fig. 6 in Young et al. 1996). As an example, a part of the simulated wave profile and the concurrent low-frequency component are presented in Fig. 11; long waves are extracted by low-pass filtering the signal with the cutoff frequency $\omega \approx 0.5\ \omega_p$. For a directional spreading corresponding to $s(\omega_p) = 11$, a setdown is usually observed under energetic groups. As the spreading becomes wider, the setdown effects reduce (cf. Dalzell 1999). However, for very broad directional distribution [i.e., $s(\omega_p) = 5$ and 3] the low-frequency component tends to raise the local mean sea level; when $s(\omega_p) = 3$, in particular, a setup can be clearly seen under the largest waves (thick solid line in Fig. 11b).

c. *Bispectra and phase relation of the low-frequency response*

The bispectrum provides a measure of the nonlinear phase coupling between wave triads with frequencies of ω_i, ω_j, and $\omega_i + \omega_j$ (Hasselmann et al. 1963), that is, two

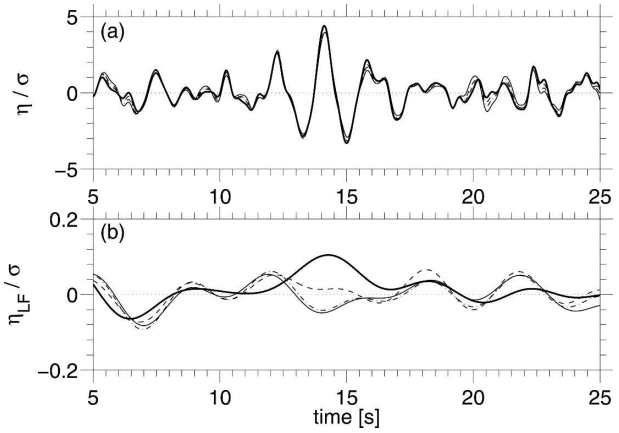

FIG. 11. (a) Second-order profile and (b) low-frequency response for progressively broader directional spectra: $s(\omega) = 11$ (solid line), $s(\omega) = 7$ (dash–dot line), $s(\omega) = 5$ (dashed line), $s(\omega) = 3$ (thick solid line). Degree of nonlinearity $\mu \approx 0.25$ and $\nu \approx 0.07$.

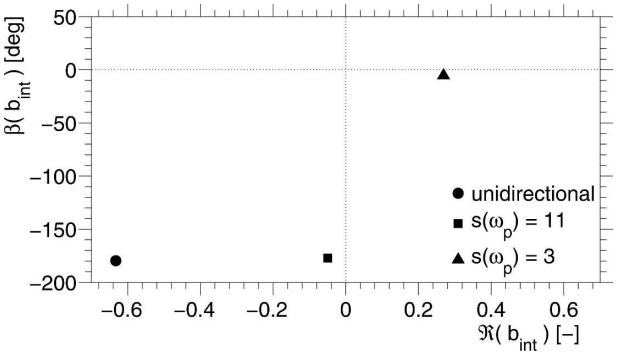

FIG. 12. Biphase (β) vs real part ($\Re$) of integrated bispectra (over all wave pairs with difference frequency $0 < \hat{\omega}E\omega^{\Gamma} < 0.5\omega_p$) from simulated second-order time series; degree of nonlinearity $\mu \approx 0.25$ ($\nu \approx 0.07$).

primary wave components forcing a secondary wave component. Here, bispectral analysis is used to investigate the contribution of the low-frequency components and the phase relation of the forced low-frequency motion, which were observed at Lake George. For discretely sampled data, the complex bispectral estimate $B(\omega_i, \omega_j)$ can be expressed in terms of Fourier coefficients (see, e.g., Haubrich 1965; Kim and Powers 1979)

$$B(\omega_i, \omega_j) = \langle F(\omega_i)F(\omega_j)F^*(\omega_i + \omega_j)\rangle, \tag{12}$$

where $\langle\rangle$ denotes an expected value, $F(\omega_i)$ is a complex Fourier coefficient, and the asterisk indicates a complex conjugate. Whereas the imaginary part of the bispectrum is related to the horizontal asymmetry of the wave profile, the real part is proportional to the skewness (i.e., vertical asymmetry; see Elgar and Guza 1985).

For the remainder of this study, we shall use a normalized form of the bispectrum; it can be written as follows (see, e.g., Kim and Powers 1979):

$$b(\omega_i, \omega_j) = \frac{B(\omega_i, \omega_j)}{\langle |F(\omega_i)F(\omega_j)|\rangle\langle |F(\omega_i + \omega_j)|\rangle}. \tag{13}$$

Phase information of the phase-coupled components can be obtained from the biphase (Kim and Powers 1979), which is defined as

$$\beta(\omega_i, \omega_j) = \arctan\left\{\frac{\Im[B(\omega_i, \omega_j)]}{\Re[B(\omega_i, \omega_j)]}\right\}, \tag{14}$$

where $\Im(\,)$ and $\Re(\,)$ are the imaginary and real parts of the bispectrum, respectively.

A measure of the nonlinear phase coupling between primary waves and low-frequency components (K^-) can be estimated by integrating the bispectrum over all wave pairs with difference frequency $\hat{\omega} = \omega_i - \omega_j$ (cf. Herbers et al. 1994), such that $0 < \hat{\omega} < 0.5\omega_p$,

$$b_{\text{int}} = 2\int_0^{0.5\omega_p} d\hat{\omega} \int_{\hat{\omega}}^{\infty} b(\omega, \hat{\omega})\, d\omega. \tag{15}$$

To understand the role of the directional distribution on the integrated bispectrum, we have first undertaken a bispectral analysis on simulated second-order wave profiles, where all energy in the low-frequency band is phase coupled. Long time series (2^{19} points) have been used to reduce the statistical uncertainty of the results. In Fig. 12, the biphase (β) and the real part ($\Re$) of the integrated bispectrum [Eq. (15)] are presented; a unidirectional case and two directional cases [$s(\omega_p) = 11$ and 3], are considered; the degree of nonlinearity is $\mu \approx 0.25$ ($\nu \approx 0.07$).

In the unidirectional case, the formation of the setdown is related to the fact that the contribution of K^- is negative; this leads to a negative value for the real part of the integrated bispectrum (cf. Okihiro et al. 1992; Herbers et al. 1994). The biphase [$\beta(b_{\text{int}})$], in this respect, shows that the low-frequency components and the group envelopes are approximately 180° out of phase. If the energy is distributed on a fairly broad directional range [$s(\omega_p) = 11$], the contribution of K^- reduces. As a result, the amplitude of the setdown reduces, and the real part of the bispectrum assumes a small, negative value [$\Re(b_{\text{int}}) \approx -0.05$]; long waves still show a phase shift of 180° relative to the group envelopes. In the case in which the directional distribution is very broad [$s(\omega_p) = 3$], however, the positive contribution of noncollinear components dominates the difference-frequency interaction, and hence a setup of the mean free surface occurs (see also Fig. 11). Conse-

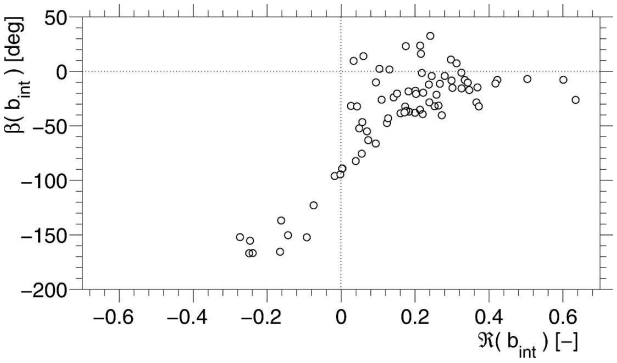

FIG. 13. Biphase (β) vs real part ($\Re$) of observed, integrated bispectra (over all wave pairs with difference frequency $0 < \hat{\omega}E\omega^{\Gamma} < 0.5\omega_p$).

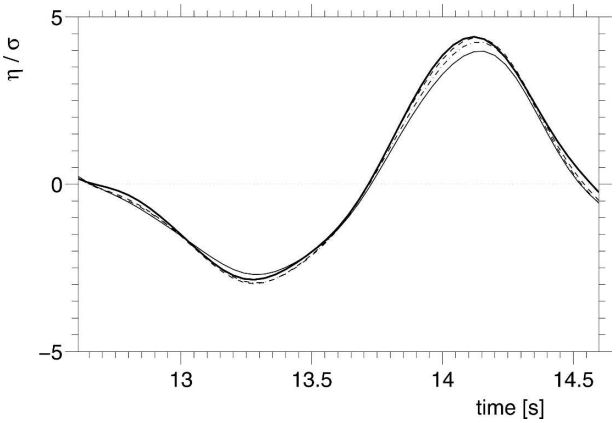

FIG. 14. Second-order wave profile: $s(\omega_p) = 11$ (solid line), $s(\omega_p) = 7$ (dash–dot line), $s(\omega_p) = 5$ (dashed line), and $s(\omega_p) = 3$ (thick solid line). Degree of nonlinearity $\mu \approx 0.25$ ($\nu \approx 0.07$).

quently, the value of the integrated bispectrum becomes positive [$\Re(b_{\text{int}}) \approx 0.27$], and the low-frequency component and the group envelopes are approximately in phase [$\beta(b_{\text{int}}) \approx 0$].

We now extend the bispectral analysis to the Lake George dataset. Long time series (2^{19} points) have been considered to perform the analysis; to this end, wave records with similar characteristics (i.e., similar H_s, T_p, and μ) have been combined. The biphase and real part of the integrated bispectra are shown in Fig. 13.

The experimental data show that the real part of the integrated bispectra assumes both negative and positive values. When $\Re(b_{\text{int}}) < 0$, the low-frequency component and the group envelopes are approximately 180° out of phase. Owing to wide directional distributions, however, the real parts of the observed, integrated bispectra can become positive, as predicted by the second-order theory. For these cases, the low-frequency response and the group envelopes are approximately in phase. This confirms, to some extent, that the formation of the setup (Figs. 6 and 7) is a statistically significant feature of the observed, bound low-frequency response.

6. Effect of setup on the wave crest distribution

For broad directional spreading, the formation of a setup produces a positive contribution to the second-order surface elevation; this may lead to an increase of the amplitude of the largest crests. In Fig. 14, we show an individual wave, corrected to the second order, which has been obtained with progressively wider directional spreading and an identical phase. For a directional distribution characterized by $s(\omega_p) = 3$, the wave crest is up to 8% higher than the one simulated with a narrower directional distribution, that is, $s(\omega_p) = 11$ [Eq. (9)].

It is now instructive to verify whether the setup changes the form of the wave crest distribution in a random wave field. An additional set of 500 random time series, therefore, have been simulated by using a modified form of the spreading function in Eq. (9), such that $s(\omega_p) = 3$; only nonlinear coefficients $\mu \geq 0.25$ ($\nu \geq 0.07$) have been considered herein. The distribution of the crest amplitude is presented in Fig. 15; it is compared with the probability density function related to a narrower directional spreading [$s(\omega_p) = 11$], which does not produce setup. Although, for a broad directional distribution, the setup contributes positively to the amplitude of the wave crests, the form of the probability density function does not change significantly. The wave crest distribution, in fact, lies within the 95% confidence limits, which are associated to the crest height distribution of a wave field with narrower directional spreading.

7. Conclusions

Simulated times series corrected to second order have been used to study the form of the wave crest distribution at different degrees of nonlinearity in a finite water depth environment. Field measurements from Lake George's instrumentation site (Australia) have been used to support this research.

The simulations have been performed by using a JONSWAP-like frequency spectrum and a $\cos{-2s}$ directional function, such that they represent an average description of the observed wave field. The statistical properties, derived from a second-order wave model, provide a good approximation of the measure-

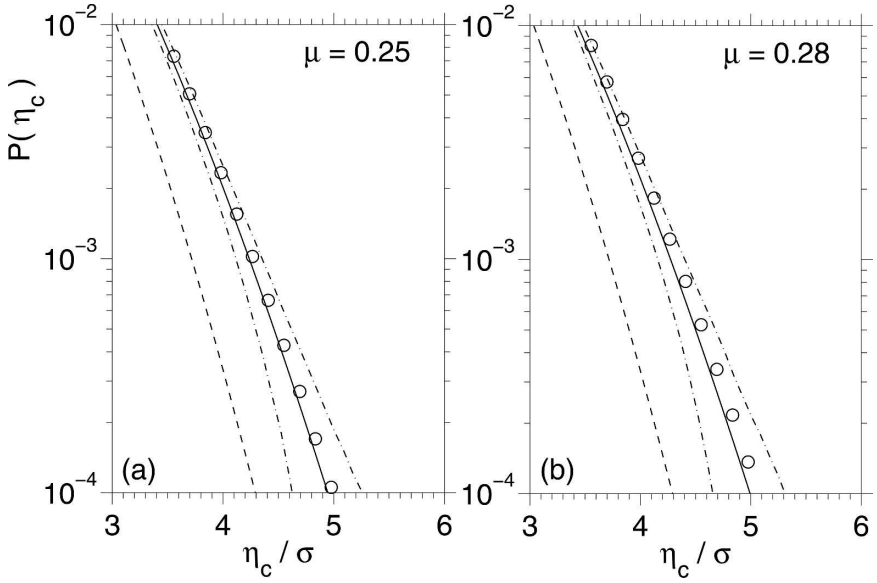

FIG. 15. Wave crest distribution of a random wave field with wide directional distribution [$s(\omega_p) = 3$] (o) compared with the Rayleigh distribution (dashed line) and the statistical distribution of a narrower directional wave field [$s(\omega_p) = 11$] (solid line); the 95% confidence limits of the latter are included (dash–dot line).

ments. However, for large degrees of nonlinearity (i.e., $\mu > 0.25$), a deviation of the observed wave crest distribution can be easily seen; such a deviation becomes statistically significant only for a value of the nonlinear coefficient of $\mu \geq 0.28$, because the contribution of the kurtosis is no longer negligible. Additional terms of a Stokes expansion will be needed for such high nonlinearity. Note also that the JONSWAP parameterization of the frequency spectrum could be inadequate in finite water depth; a slightly different form of the probability distribution might be obtained if, for example, a TMA spectral parameterization would be used. Further investigations are needed to clarify this.

At the second order in nonlinearity, it is usually expected that long-wave components produce a setdown of the mean sea level under the most energetic wave groups. The analysis of field measurements, however, indicates that low-frequency components can sometimes generate a setup when a wide spreading characterizes the directional distribution. A numerical study of the coupling coefficients, in this respect, shows that this result is consistent with the second-order theory; the second-order difference contribution, which is responsible for the formation of the setdown, becomes positive when the interacting wave components travel along well-separated directions. Repeating the simulation with a progressively broader directional distribution confirms the generation of a local increase of the mean sea level under energetic groups. Note, however, that because of the particular geometrical characteristics of the measurement sites, effects of reflected free infragravity waves on the formation of the setup may not be excluded a priori. An analysis of the spectral energy over the infragravity frequency band show that free infragravity waves only have a marginal influence for the formation of the observed setup. A bispectral analysis over the low-frequency band, furthermore, confirms that the formation of the setup resulting from bound long waves is a statistically significant feature of the observed records.

If a setup replaces the expected setdown, the amplitude of an individual wave crest may increase, because of the positive contribution of the low-frequency components. Nonetheless, a broad directional distribution does not significantly change the form of the probability density function; at least, not at the degrees of nonlinearity and level of probability considered in this study.

Acknowledgments. This work was carried out in the framework of the FWO project G.0228.02 and G.0477.04, and the EU project SEAMOCS (Contract MRTN-CT-2005-019374). The numerical simulations were performed by using the K.U. Leuven's High Performing Computing (HPC) facilities. Onorato was supported by MIUR (PRIN project). The manuscript has

benefited from the detailed comments and suggestions provided by the anonymous referees.

APPENDIX

Coupling Coefficients

Here we report the analytical form of the coupling coefficients of the second-order theory:

$$K^{+}_{ijlm} = \{D^{+}_{ijlm} - [k_i k_j \cos(\theta_l - \theta_m) - R_i R_j]\}(R_i R_j)^{-1/2} + (R_i + R_j) \quad \text{and} \tag{A1}$$

$$K^{-}_{ijlm} = \{D^{-}_{ijlm} - [k_i k_j \cos(\theta_l - \theta_m) - R_i R_j]\}(R_i R_j)^{-1/2} + (R_i + R_j), \tag{A2}$$

where

$$D^{+}_{ijlm} = \frac{(\sqrt{R_i} + \sqrt{R_j})[\sqrt{R_i}(k_j^2 - R_j^2) + \sqrt{R_j}(k_i^2 - R_i^2)]}{(\sqrt{R_i} + \sqrt{R_j})^2 - k^{+}_{ijlm}\tanh(k^{+}_{ijlm}h)} + \frac{2(\sqrt{R_i} + \sqrt{R_j})^2[k_i k_j \cos(\theta_l - \theta_m) - R_i R_j]}{(\sqrt{R_i} + \sqrt{R_j})^2 - k^{+}_{ijlm}\tanh(k^{-}_{ijlm}h)}, \tag{A3}$$

$$D^{-}_{ijlm} = \frac{(\sqrt{R_i} - \sqrt{R_j})[\sqrt{R_i}(k_i^2 - R_i^2) - \sqrt{R_i}(k_j^2 - R_j^2)]}{(\sqrt{R_i} - \sqrt{R_j})^2 - k^{-}_{ijlm}\tanh(k^{-}_{ijlm}h)} + \frac{2(\sqrt{R_i} - \sqrt{R_j})^2[k_i k_j \cos(\theta_l - \theta_m) - R_i R_j]}{(\sqrt{R_i} - \sqrt{R_j})^2 - k^{-}_{ijlm}\tanh(k^{-}_{ijlm}h)}, \tag{A4}$$

$$k^{-}_{ijlm} = \sqrt{k_i^2 + k_j^2 - 2k_i k_j \cos(\theta_l - \theta_m)}, \tag{A5}$$

$$k^{+}_{ijlm} = \sqrt{k_i^2 + k_j^2 + 2k_i k_j \cos(\theta_l - \theta_m)}, \tag{A6}$$

and

$$R_i = \omega_i^2/g. \tag{A7}$$

REFERENCES

Battjes, J., H. Bakkenes, T. Janssen, and A. van Dongeren, 2004: Shoaling of subharmonic gravity waves. *J. Geophys. Res.,* **109,** C02009, doi:10.1029/2003JC001863.

Bouws, E., H. Günther, W. Rosenthal, and C. Vincent, 1985: Similarity of the wind wave spectrum in finite depth water. 1. Spectral form. *J. Geophys. Res.,* **90,** 975–986.

Dalzell, J., 1999: A note on finite depth second-order wave-wave interactions. *Appl. Ocean Res.,* **21,** 105–111.

Elgar, S., and R. T. Guza, 1985: Observations of bispectra of shoaling surface gravity waves. *J. Fluid Mech.,* **161,** 425–448.

Emery, W. J., and R. E. Thomson, 2001: *Data Analysis Methods in Physical Oceanography*. 2d ed. Elsevier, 638 pp.

Forristall, G. Z., 2000: Wave crest distributions: Observations and second-order theory. *J. Phys. Oceanogr.,* **30,** 1931–1943.

Goda, Y., 2000: *Random Seas and Design of Maritime Structures*. P. L.-F. Liu, Ed., Advanced Series on Ocean Engineering, Vol. 15, World Scientific, 443 pp.

Hasselmann, K., 1962: On the non-linear energy transfer in a gravity-wave spectrum. Part I: General theory. *J. Fluid Mech.,* **12,** 481–500.

——, W. Munk, and G. MacDonald, 1963: Bispectra of ocean waves. *Time Series Analysis,* M. Rosenblatt, Ed., John Wiley and Sons, 125–139.

Haubrich, R. A., 1965: Earth noise, 5 to 500 millicycles per second. I. Spectral stationarity normality and nonlinearity. *J. Geophys. Res.,* **70,** 1415–1427.

Hauser, D., K. K. Kahma, H. E. Krogstad, S. Lehner, J. Monbaliu, and L. R. Wyatt, Eds., 2005: *Measuring and Analysing the Directional Spectrum of Ocean Waves*. COST, 465 pp.

Haver, S., and J. Andersen, 2000: Freak waves: Rare realizations of a typical population or typical realizations of a rare population? *Proc. 10th Int. Conf. on Offshore and Polar Engineering,* Seattle, WA, ISOPE, 123–130.

Herbers, T. H., S. Elgar, and R. T. Guza, 1994: Infragravity-frequency (0.005–0.05 hz) motions on the shelf. Part I: Forced waves. *J. Phys. Oceanogr.,* **24,** 917–927.

——, ——, ——, and W. C. O'Reilly, 1995: Infragravity-frequency (0.005–0.05 hz) motions on the shelf. Part II: Free waves. *J. Phys. Oceanogr.,* **25,** 1063–1079.

IAHR Working Group on Wave Generation and Analysis, 1986: List of sea-state parameters. *J. Waterw., Port, Coastal, Ocean Eng.,* **115,** 793–808.

Janssen, P. A. E. M., 2003: Nonlinear four-wave interactions and freak waves. *J. Phys. Oceanogr.,* **33,** 863–884.

——, and M. Onorato, 2005: The shallow water limit of the Zakharov equation and consequences of (freak) wave prediction. ECMWF Tech. Memo. 464, European Centre for Medium-Range Weather Forecasts, Reading, United Kingdom, 15 pp.

Jensen, J. J., 2005: Conditional second-order short-crested water waves applied to extreme wave episode. *J. Fluid Mech.,* **545,** 29–40.

Kim, Y. C., and E. J. Powers, 1979: Digital bispectral analysis and its applications to nonlinear wave interactions. *IEEE Trans. Plasma Sci.,* **7,** 120–131.

Komen, G. J., L. Cavaleri, M. Donelan, K. Hasselmann, S. Hasselmann, and P. A. E. M. Janssen, 1994: *Dynamics and Modelling of Ocean Waves.* Cambridge University Press, 532 pp.

Longuet-Higgins, M. S., 1963: The effect of non-linearities on statistical distributions in the theory of sea waves. *J. Fluid Mech.,* **17,** 459–480.

——, and R. W. Stewart, 1962: Radiation stress and mass transport in gravity waves, with application to "surf beats." *J. Fluid Mech.,* **13,** 481–504.

—— and ——, 1964: Radiation stresses in water waves: A physical discussion with applications. *Deep-Sea Res.,* **11,** 529–562.

Martinsen, T., and S. R. Winterstein, 1992: On the skewness of random surface waves. *Proc. Second Int. Conf. on Offshore and Polar Engineering,* Vancouver, BC, Canada, ISOPE, 472–478.

Mori, N., and P. A. E. M. Janssen, 2006: On kurtosis and occurrence probability of freak waves. *J. Phys. Oceanogr.,* **36,** 1471–1483.

Nieto-Borge, J. C., S. Lehner, T. Schneiderhan, J. Schulz-Stellenfleth, and A. Niedermeier, 2004: Use of spaceborne synthetic aperture radar for offshore wave analysis. *Proc. 23rd Int. Conf. on Offshore Mechanics and Arctic Engineering,* Vancouver, BC, Canada, OMAE, CD-ROM, OMAE2004-51588.

Ochi, M. K., 1998: *Ocean Waves: The Stochastic Approach.* Cambridge University Press, 319 pp.

Okihiro, M., R. T. Guza, and R. J. Seymour, 1992: Bound infragravity waves. *J. Geophys. Res.,* **97,** 11 453–11 469.

Onorato, M., A. Osborne, M. Serio, L. Cavaleri, C. Brandini, and C. Stansberg, 2006: Extreme waves, modulational instability and second order theory: Wave flume experiments on irregular waves. *Eur. J. Mech.,* **25,** 586–601.

Osborne, A. R., and M. Petti, 1994: Laboratory-generated, shallow-water surface waves: Analysis using the periodic, inverse scattering transform. *Phys. Fluids,* **6,** 1727–1744.

Prevosto, M., H. E. Krogstad, and A. Robin, 2000: Probability distributions for maximum wave and crest heights. *Coastal Eng.,* **40,** 329–360.

Sharma, N., and R. Dean, 1981: Second-order directional seas and associated wave forces. *Soc. Petrol. Eng. J.,* **4,** 129–140.

Socquet-Juglard, H., K. Dysthe, K. Trulsen, H. E. Krogstad, and J. Liu, 2005: Probability distributions of surface gravity waves during spectral changes. *J. Fluid Mech.,* **542,** 195–216.

Tayfun, A. M., 1980: Narrow-band nonlinear sea waves. *J. Geophys. Res.,* **85,** 1548–1552.

Toffoli, A., M. Onorato, and J. Monbaliu, 2006: Wave statistics in unimodal and bimodal seas from a second-order model. *Eur. J. Mech.,* **25,** 649–661.

Ursell, F., 1953: The long wave paradox in the theory of gravity waves. *Proc. Cambridge Philos. Soc.,* **49,** 685–694.

Walker, D. A. G., P. H. Taylor, and R. E. Taylor, 2004: The shape of large surface waves on the open sea and the Draupner New Year wave. *Appl. Ocean Res.,* **26,** 73–83.

Whitham, G. B., 1974: *Linear and Nonlinear Waves*. Wiley, 636 pp.

Young, I. R., L. A. Verhagen, and S. K. Khatri, 1996: The growth of fetch limited waves in water depth of finite depth. Part 3. Directional spectra. *Coastal Eng.,* **29,** 101–121.

——, M. L. Banner, M. A. Donelan, A. V. Babanin, W. Melville, F. Veron, and C. McCormick, 2005: An integrated system for the study of wind-wave source terms in finite-depth water. *J. Atmos. Oceanic Technol.,* **22,** 814–831.